PSILOGOS

Research Article

open-access

Topology-Constrained Regional Attenuation Identifies a Posterior Associative Core in Schizophrenia

Kishore Mahbubani

ABSTRACT

Regional amplitude of low-frequency fluctuation (ALFF) abnormalities in schizophrenia are often interpreted one region at a time, even though the implicated areas differ in effect magnitude, spatial extent, anatomical position, and classification behavior. The present study asked whether these dimensions converge on a stable distributed phenotype and whether that phenotype is concentrated in posterior association cortex. Resting-state functional magnetic resonance imaging measurements from 131 adults with schizophrenia and 128 healthy participants yielded seven regions with lower ALFF: bilateral precuneus, left angular gyrus, bilateral middle temporal gyri, left anterior cingulate cortex, left fusiform gyrus, and right cerebellum. Acquisition, preprocessing, voxelwise comparison, support vector classification, and receiver-operating-characteristic procedures were retained. A topology-constrained regional evidence method was added. It combined percentile scores for attenuation magnitude, cluster extent, peak classification accuracy, and Gaussian distance-kernel centrality. Equal-weight scores were examined together with 200,000 Dirichlet-distributed weight vectors, leave-one-criterion analyses, posterior evidence-share estimation, summary-statistic demographic tests, and decision-balance calculations. The bilateral precuneus ranked first (score 0.875) and the left angular gyrus ranked second (0.768). The precuneus occupied rank 1 in 79.4% of weight draws, while the angular gyrus did so in 20.0%. Posterior association regions accounted for 70.5% of equal-weight evidence; their median share over the weight simplex was 70.8% (central 95% range 64.5–75.8%). Excluding any one criterion preserved the ordering strongly (Spearman $\rho = 0.883$–0.982). The patient group was younger by 3.99 years (Hedges $g = -0.43$), whereas education was comparable. Precuneus and angular-gyrus decision profiles had nearly identical balanced accuracy (73.15% and 73.12%) despite different sensitivity–specificity combinations. Schizophrenia-related ALFF attenuation is best characterized as a stable posterior associative pattern led by the precuneus and angular gyrus, not as an isolated single-locus effect. Its regional ordering is robust to evidence preferences, but demographic imbalance and modest specificity restrict individual diagnostic interpretation.

Keywords: schizophrenia; resting-state fMRI; amplitude of low-frequency fluctuation; precuneus; angular gyrus; regional topology; robustness analysis

Department of Psychological Medicine, Yong Loo Lin School of Medicine, National University of Singapore, Singapore
kishmahubani45@gamil.com

– **Published:** 5 November 2024

1. INTRODUCTION

Schizophrenia is a severe psychiatric disorder whose clinical expression encompasses psychosis, disorganization, negative symptoms, cognitive impairment, and functional decline. The syndrome is heterogeneous in onset, course, treatment response, and disability, so a diagnostic label does not identify a single neural disturbance. Contemporary accounts therefore describe schizophrenia as a disorder of interacting molecular, cellular, and systems-level processes rather than a lesion confined to one anatomical site.[1–3] Clinical diagnosis remains indispensable, yet it is based on observed behavior and reported experience. Objective measurements may complement that process by clarifying mechanisms, separating sources of heterogeneity, and quantifying treatment-related change. The long search for a stand-alone diagnostic marker has nevertheless produced limited clinical translation, partly because statistical group separation is often mistaken for reliable individual identification.[4]

Systems neuroscience offers several reasons to expect distributed rather than focal alterations. Dopaminergic and glutamatergic disturbances affect synaptic gain, plasticity, and the coordination of neuronal ensembles across multiple circuits.[5] Dysconnection accounts similarly propose that symptoms arise when specialized regions cannot exchange or contextualize information appropriately.[6] Oscillatory abnormalities provide a related temporal account: deficient synchronization can impair the integration of local computations over the spatial and temporal scales needed for perception, working memory, and self-monitoring.[7] These positions differ in biological level, but each predicts that a useful imaging phenotype should be evaluated as a pattern whose parts vary in strength, anatomical reach, and functional role.

Resting-state functional magnetic resonance imaging (rs-fMRI) is well suited to measuring such distributed physiology because it records spontaneous blood-oxygen-level-dependent variation without imposing a task that may be performed differently by patients and controls. Quantitative synthesis has identified convergent resting abnormalities while also showing substantial regional and analytical heterogeneity.[8,9] Work in schizophrenia has repeatedly implicated medial prefrontal, posterior cingulate, precuneus, lateral parietal, temporal, and frontoparietal territories. Altered default-network coupling has been related to internally directed cognition and psychopathology,[10] while resting connectivity differences have been associated with cognitive performance.[11] The default network is not a unitary idle system; it contains interacting subsystems that participate in autobiographical memory, semantic construction, social cognition, and shifts between internally and externally oriented processing.[12,13] A posterior pattern that spans the precuneus, angular gyrus, and temporal cortex may therefore reflect impaired integration among complementary operations rather than redundant manifestations of the same abnormality.

The anatomy of the implicated posterior regions sharpens this hypothesis. The precuneus occupies medial parietal cortex and participates in episodic retrieval, visuospatial imagery, self-related processing, and conscious representation.[14] Its extensive connections allow it to coordinate medial temporal, lateral parietal, frontal, and subcortical activity. The angular gyrus lies at the convergence of visual, somatosensory, auditory, and language-related streams. It supports semantic combination, episodic recollection, number processing, attention reorientation, and aspects of social inference.[15] Meta-analytic evidence places the angular and middle temporal gyri within a distributed semantic system.[16] Resting disturbances across these areas are also relevant to auditory verbal hallucinations, which have been linked to altered intrinsic communication among temporal, parietal, and monitoring systems.[17] A joint posterior alteration could consequently affect how internally generated content acquires meaning, certainty, and perceived external origin.

ALFF provides a regional measure of spontaneous signal magnitude. The procedure transforms each voxel time series to the frequency domain and summarizes the square root of power within a low-frequency interval. Fractional ALFF was later introduced to reduce sensitivity to physiological components outside the selected band,[18] and percent-amplitude formulations have been proposed to improve interpretability across voxels and samples.[19] Although ALFF does not directly measure neuronal firing, convergent physiological work supports its value as an index of regional resting fluctuation when acquisition, motion, nuisance regression, filtering, and spatial smoothing are handled carefully. Its appeal in schizophrenia is conceptual as well as practical: it can identify regional amplitude attenuation without first specifying a seed or imposing a network parcellation.

Prior rs-fMRI investigations have produced several candidate signatures. Striatal functional abnormalities have shown value for hypothesis-driven individual classification.[20] Regional insular volume reductions have been observed in drug-naive first-episode patients and unaffected siblings,[21] while anterior cingulate connectivity has been associated with early treatment response.[22] Meta-analysis of regional resting activity has identified reproducible alterations in precuneus, frontal, temporal, and sensorimotor territories across first-episode and chronic illness.[23] Additional findings include abnormal spontaneous activity in treatment-naive schizophrenia,[24] altered right-precuneus connectivity related to cognition and depressive status,[25] disrupted angular-gyrus asymmetry,[26] and planum-temporale connectivity reductions relevant to language lateralization.[27] Taken together, these observations favor a distributed physiological account but do not establish how regional findings should be prioritized when effect magnitude, cluster size, location, and classification behavior disagree.

That disagreement is important. The largest cluster need

not show the strongest attenuation. A region that separates groups with high sensitivity may have low specificity, and a spatially central locus may exert integrative importance despite a modest univariate statistic. Selecting a region from any one of these quantities discards the other evidence. It also encourages unstable rankings because each measure occupies a different scale. The inferential issue is compounded by known rs-fMRI vulnerabilities. Head motion can generate spatially structured associations that resemble neural organization;[28] alternative motion-control procedures vary in efficacy and reliability;[29] and cluster-extent inference is sensitive to the chosen voxel threshold and smoothness assumptions.[30] Nonparametric spatial testing offers stronger control under fewer distributional assumptions when full images are available.[31] A regional synthesis should therefore make its weighting rules explicit and should quantify how conclusions change when those rules change.

Classification adds another layer of uncertainty. Support vector machines can estimate a separating boundary in high-dimensional space and have been widely applied to neuroimaging.[32] However, apparent accuracy can be optimistic when feature selection precedes data partitioning, parameter tuning is not nested, or sample size is limited relative to heterogeneity. Careful cross-validation design is essential for brain decoders,[33] and small samples can produce wide uncertainty even when mean performance appears acceptable.[34,35] Predictive studies should report sensitivity and specificity alongside accuracy, retain all feature-selection steps within resampling, and evaluate transport to independent sites.[36] Transparent computation and complete reporting are likewise necessary if a regional signature is to be independently checked.[37]

The present study addressed a different question from conventional single-region discrimination: do multiple dimensions of regional evidence converge on a stable schizophrenia-related attenuation architecture, and is that architecture preferentially concentrated in posterior association cortex? A topology-constrained regional evidence strategy was devised to answer that question. Four normalized criteria were combined: absolute group contrast, cluster extent, peak univariate classification accuracy, and spatial centrality obtained from interregional MNI distances. Weighted-sum analysis is interpretable but can depend on the chosen weights;[38] accordingly, the full admissible weight simplex was sampled rather than relying only on equal weights. Centrality was treated as a local property of distance-weighted relations, consistent with the principle that a node's importance depends on the flows or contacts represented by its edges.[39] The study also audited demographic comparability using effect sizes[40] and decomposed posterior decision performance into sensitivity, specificity, balanced accuracy, and Youden index. The primary hypothesis was that precuneus and angular-gyrus attenuation would occupy the most stable ranks and that posterior associative regions would retain more than half of total evidence across plausible criterion preferences.

2. MATERIALS AND METHODS

The analysis used a cohort of 259 adults: 131 patients who met DSM-IV criteria for schizophrenia and 128 age- and sex-matched healthy participants. The patient group included 76 men and 55 women; the control group included 75 men and 53 women. Mean age was 26.34 years (SD 10.39) in patients and 30.33 years (SD 7.90) in controls. Mean education was 9.50 years (SD 2.64) and 9.30 years (SD 2.61), respectively. Patients had a mean onset age of 19.42 years (SD 12.21), mean illness duration of 6.92 years (SD 4.86), mean Positive and Negative Syndrome Scale score of 89.63 (SD 17.00), and mean Repeatable Battery for the Assessment of Neuropsychological Status score of 177.61 (SD 38.60). The cohort, scanning parameters, and seven regional cluster summaries were transcribed from the open-access report by Gao and colleagues;[41] that article is the sole provenance citation for these measurements.

The analytic dataset differed in unit and purpose from an individual-image classification table. Each row represented one statistically attenuated region, and each column encoded a distinct property of that region: MNI peak coordinate, cluster extent, voxelwise t statistic, and peak univariate classification accuracy. The seven rows were right cerebellum, left middle temporal gyrus, right middle temporal gyrus, left fusiform gyrus, left anterior cingulate cortex, bilateral precuneus, and left angular gyrus. This regional matrix was used to test convergence, dominance, and robustness. Patient-level prediction was not recomputed because individual images and fold assignments were not available; consequently, all new ranking claims concern regional evidence rather than unseen-person diagnosis.

2.1. Participants, acquisition, and established signal analyses

Participants were 18–64 years old, right-handed, and free of neurological disease, severe medical illness, substance abuse, and electroconvulsive therapy. Schizophrenia was diagnosed independently by two psychiatrists after a structured Chinese MINI interview and confirmed after three months. Symptoms and cognition were assessed before scanning with Chinese PANSS and RBANS instruments. Healthy participants had no severe medical or neuropsychiatric history and no first-degree family history of neuropsychiatric illness. Written consent and local ethics approval were obtained for the clinical investigation.

Resting images were acquired on a Philips Ingenia 3.0 T system using gradient-echo echo-planar imaging. The principal parameters were repetition time 2000 ms, echo time 30 ms, 35 slices, 64×64 matrix, flip angle 78°, 22.4 cm field of view, 3.5 mm slice thickness, and 0.6 mm interslice gap. Participants kept their eyes closed, remained awake, and avoided deliberate mental activity.

A T1-weighted anatomical volume was acquired with 1 mm thickness, no interslice gap, repetition time 8.4 ms, echo time 3.2 ms, and 256×256 field of view. Five participants initially exceeded motion limits and were rescanned on the same day.

The first ten functional volumes were discarded. Remaining volumes underwent slice-time correction, rigid-body motion correction, coregistration with T1 anatomy, normalization to MNI space, resampling to $3 \times 3 \times 3$ mm, linear detrending, nuisance regression for white-matter and ventricular signals, temporal filtering from 0.01 to 0.08 Hz, and 6 mm full-width-at-half-maximum Gaussian smoothing. Scans had to remain within 2 mm translation and 2° rotation on every axis. ALFF was calculated by Fourier-transforming each voxel time series, taking the square root of the power spectrum, and averaging within 0.01–0.08 Hz. Group differences were assessed voxelwise with age, sex, education, and framewise displacement as covariates. The retained regional results passed Gaussian random-field cluster correction with a voxel threshold of $p < 0.01$.

Support vector classification was implemented with LIBSVM after abnormal regions had been identified. Parameter combinations were searched by cross-validation, and the highest cross-validated accuracy was recorded for each region. Receiver-operating-characteristic analysis was used for the bilateral precuneus and left angular gyrus. These established procedures were retained because they supplied complementary properties for the regional matrix. They were not treated as interchangeable: the t statistic quantified group separation, voxel count quantified spatial extent, and peak accuracy quantified univariate classification behavior.

2.2. Topology-constrained regional evidence method

Let region i have coordinate vector $\mathbf{x}_i = (x_i, y_i, z_i)$. Euclidean peak-to-peak distance was

$$d_{ij} = \left\| \mathbf{x}_i - \mathbf{x}_j \right\|_2 . \tag{1}$$

This quantity does not assert direct axonal connectivity. It supplies a reproducible anatomical proximity relation among the seven observed peaks. The median of all nonzero pairwise distances, $\sigma = 79.66$ mm, defined the scale of a Gaussian kernel,

$$A_{ij} = \exp\left(-\frac{d_{ij}^2}{2\sigma^2} \right), \qquad A_{ii} = 0. \tag{2}$$

The spatial centrality of region i was the mean of its six off-diagonal kernel weights. A high value indicates that the peak occupies a relatively central position within the observed constellation; it does not imply causal control or dense tract connectivity.

Four criteria were oriented so that a larger value represented stronger evidence: absolute t magnitude, $\log(1 +$ voxel count$)$, peak classification accuracy, and kernel centrality. Each criterion was converted to a percentile rank among seven regions. Ties received their average rank. This transformation preserved within-criterion order while preventing a quantity measured in voxels from dominating another measured in percentage points. For criterion percentile q_{ik} and nonnegative weight w_k, the regional evidence score was

$$R_i(\mathbf{w}) = \sum_{k=1}^{4} w_k q_{ik}, \qquad \sum_{k=1}^{4} w_k = 1. \tag{3}$$

The primary score used $w_k = 0.25$ for all criteria. This equal-weight estimate is deliberately transparent: each dimension contributes one quarter, and no fitted coefficient is interpreted as biological truth. Because a weighted sum can conceal preference dependence, equal weighting was treated as a reference point rather than the only admissible choice.

2.3. Preference uncertainty and criterion ablation

Uncertainty about criterion importance was represented by 200,000 weight vectors drawn from a symmetric Dirichlet distribution, $\mathbf{w} \sim \mathrm{Dirichlet}(1, 1, 1, 1)$. This distribution samples the interior of the four-dimensional simplex uniformly and allows every criterion to range from negligible to dominant. For every draw, the seven regions were sorted by $R_i(\mathbf{w})$. Win probability was the proportion of draws at rank 1; top-three probability was the proportion at ranks 1–3; and mean rank summarized the entire ordering distribution. A fixed random seed of 20260814 makes the computation exactly repeatable.

Criterion ablation removed one of the four evidence dimensions, recomputed the mean of the remaining three, and compared the resulting rank order with the complete equal-weight order using Spearman correlation. Four correlations therefore quantified the consequence of omitting attenuation, extent, classification, or centrality. Values close to one indicate that the ordering is not carried by a single criterion.

The posterior associative subset comprised bilateral precuneus, left angular gyrus, and bilateral middle temporal gyri. For each weight vector, its evidence share was

$$P(\mathbf{w}) = \frac{\sum_{i \in \mathcal{P}} R_i(\mathbf{w})}{\sum_{i=1}^{7} R_i(\mathbf{w})}, \tag{4}$$

where $\mathcal{P}$ denotes the four posterior regions. The equal-weight share, median over random weights, and central 95% interval were recorded. The interval describes preference sensitivity rather than sampling error; it asks how much the posterior conclusion changes when an analyst values the four evidence dimensions differently.

2.4. Demographic audit and decision balance

Welch tests were reconstructed from the reported sample sizes, means, and standard deviations for age and edu-

cation. Mean differences, 95% confidence intervals, two-sided p values, and Hedges g were calculated. Hedges correction was used because it removes small-sample bias from Cohen's standardized mean difference, although the correction is minor at this cohort size. The sex distributions were inspected descriptively because the proportions were nearly identical.

For the two posterior candidate regions with reported sensitivity and specificity, balanced accuracy was $(\text{sensitivity} + \text{specificity})/2$, and Youden J was $\text{sensitivity} + \text{specificity} - 100$ when quantities were expressed as percentages. These measures prevent a high true-positive rate from obscuring a weak true-negative rate. No threshold was declared clinically acceptable because the consequences of false-positive and false-negative decisions depend on the intended use and clinical setting.

3. RESULTS

The cohort contained 259 participants with nearly identical sex distributions: men represented 58.0% of patients and 58.6% of controls. Education differed by only 0.20 years. Patients were younger on average, a contrast examined formally below. Clinical scores indicated a symptomatic patient sample with substantial cognitive burden, although the absence of control PANSS and RBANS values precluded between-group comparison on those instruments. The cohort characteristics are given in table 1.

The values in table 1 establish two boundaries for inference. First, findings pertain to relatively young adults with an average illness duration of approximately seven years rather than to late-life or prodromal populations. Second, the age separation is large enough to require explicit qualification even though age was included as a voxelwise covariate. Covariate adjustment reduces linear age-related group bias in the ALFF comparison, but it cannot demonstrate that nonlinear aging effects, age-by-diagnosis interactions, or unequal age variance were absent.

All seven significant clusters showed lower ALFF in patients; no region showed an increase. Absolute t values ranged from 7.38 in right cerebellum to 8.75 in bilateral precuneus, and extents ranged from 41 voxels in left fusiform gyrus to 460 voxels in left angular gyrus. Peak accuracy ranged from 69.11% to 73.36%. The coordinates cover medial posterior, lateral posterior, temporal, ventral temporal, anterior medial, and cerebellar positions, making the finding anatomically distributed despite its posterior concentration.

The acquisition view in figure 1a provides the physical context for an eyes-closed resting examination, while figure 1b displays the observed MNI peaks without reproducing a thresholded slice mosaic. The coordinate field shows that angular-gyrus, precuneus, and temporal peaks occupy distinct locations rather than one contiguous posterior mass. Marker-size differences also reveal why extent alone would favor the angular gyrus, whereas marker color shows that attenuation magnitude favors the precuneus. The anterior cingulate lies apart along the anterior–posterior axis, and the cerebellar peak is separated inferiorly. These relations motivate the distance term used in the regional score.

3.1. Regional evidence ordering

The equal-weight method ranked bilateral precuneus first with a score of 0.875 and left angular gyrus second with 0.768. Left middle temporal gyrus ranked third at 0.625, followed by right middle temporal gyrus at 0.554, left anterior cingulate at 0.500, left fusiform at 0.429, and right cerebellum at 0.250. Thus, three of the four highest positions belonged to posterior association cortex, and all four posterior regions lay above the cerebellum. The complete values appear in table 2.

The pattern in table 2 explains why the top two regions are not interchangeable. The angular gyrus has the largest cluster and ties for the greatest peak accuracy, but its attenuation magnitude is lower than that of the precuneus. The precuneus combines the strongest attenuation, a large cluster, maximal accuracy, and high spatial centrality. Its leading score therefore reflects concordance across evidence dimensions. By contrast, the cerebellar region is small, has the weakest attenuation, and has the lowest classification accuracy; anatomical remoteness further lowers its centrality. The method does not erase cerebellar involvement, but it distinguishes presence of an abnormality from priority within the observed constellation.

The scatter in figure 2a places precuneus and angular gyrus at the high-accuracy edge but separates them by attenuation magnitude and extent. Middle temporal regions occupy intermediate positions, while fusiform and cerebellar clusters show lower joint evidence. The profile display in figure 2b reveals the source of each combined score. Precuneus is consistently high; angular gyrus is strong in extent and classification but weaker in centrality; left fusiform has low attenuation, extent, and classification ranks yet unusually high centrality. That fusiform configuration is important because it shows how a region can become competitive under a preference that strongly favors spatial position, a possibility quantified by the weight experiment.

3.2. Weight uncertainty and criterion ablation

Across 200,000 random weight vectors, bilateral precuneus ranked first in 79.37% of draws and remained in the top three in every draw. Left angular gyrus ranked first in 20.02% and appeared in the top three in 92.69%. Left fusiform won 0.61% of draws when centrality received extreme weight; no other region won. Left middle temporal gyrus entered the top three in 59.36% of draws, right middle temporal gyrus in 23.47%, anterior cingulate in 13.63%, and right cerebellum in none. Mean ranks

Table 1. Participant characteristics.

Characteristic	Schizophrenia ($n = 131$)	Control ($n = 128$)
Male/female	76/55	75/53
Age, years	26.34 ± 10.39	30.33 ± 7.90
Education, years	9.50 ± 2.64	9.30 ± 2.61
Age at onset, years	19.42 ± 12.21	–
Illness duration, years	6.92 ± 4.86	–
PANSS total	89.63 ± 17.00	–
RBANS total	177.61 ± 38.60	–

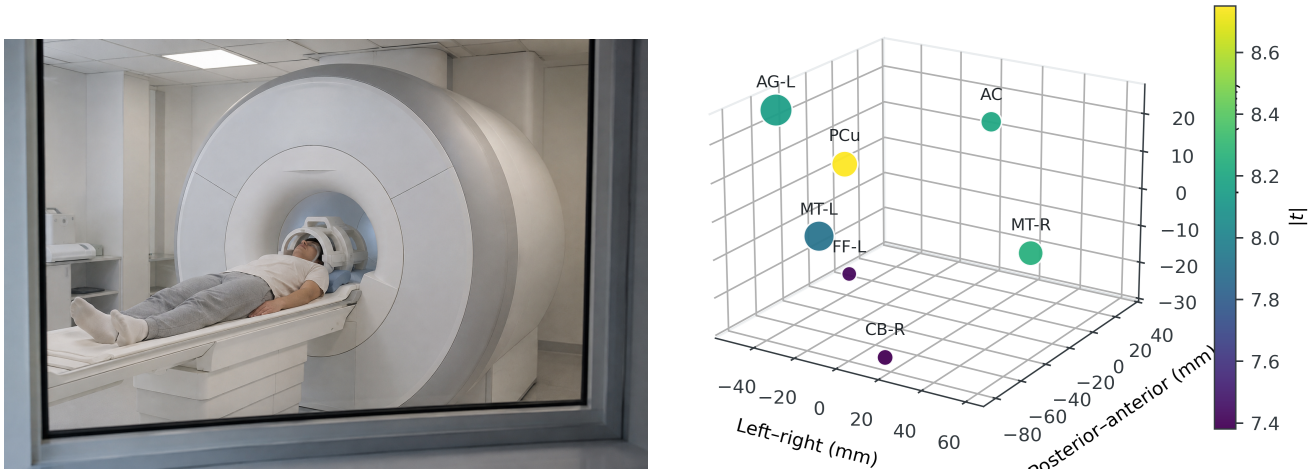

(a) Illustrative acquisition context.

(b) Regional coordinate distribution.

Figure 1. Acquisition and spatial distribution.

Table 2. Regional attenuation and topology scores.

Region	x	y	z	Voxels	t	Accuracy (%)	Evidence score
Right cerebellum	18	-81	-27	58	-7.38	69.11	0.250
Left middle temporal	-51	-24	-15	399	-7.91	70.27	0.625
Right middle temporal	60	-39	-3	246	-8.25	70.27	0.554
Left fusiform	-30	-33	-21	41	-7.41	69.88	0.429
Left anterior cingulate	0	33	12	148	-8.20	70.66	0.500
Bilateral precuneus	-6	-72	18	273	-8.75	73.36	0.875
Left angular	-51	-54	24	460	-8.15	73.36	0.768

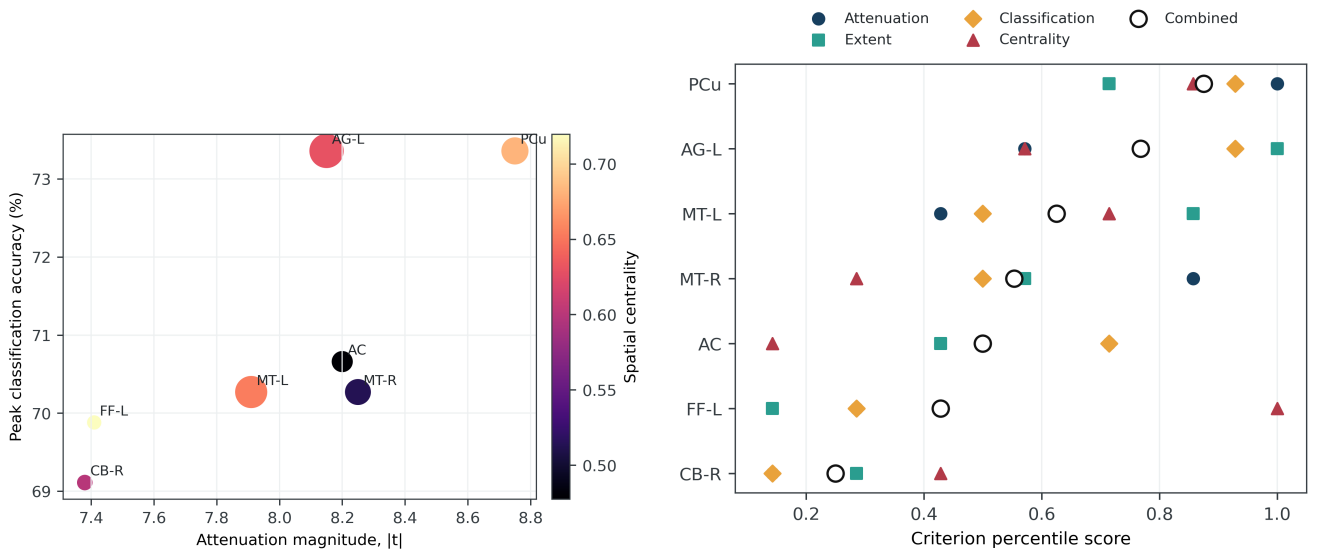

(a) Joint evidence plane.

(b) Criterion profiles.

Figure 2. Regional evidence structure.

were 1.23 for precuneus, 2.04 for angular gyrus, 3.58 for left middle temporal gyrus, 4.12 for right middle temporal gyrus, 4.91 for anterior cingulate, 5.26 for fusiform, and 6.86 for cerebellum.

The probabilities in table 3 show that the primary conclusion is not an artifact of equal weights. The only consequential exchange occurs between the leading posterior regions, with a small corner of weight space favoring fusiform centrality. Excluding extent produced the highest agreement with the complete ranking ($\rho = 0.982$), indicating that extent added little unique ordering information. Excluding classification also preserved the ranks closely ($\rho = 0.964$). Attenuation and centrality had larger, though still modest, effects on ordering ($\rho = 0.883$ and 0.893). No omission reversed the broad posterior dominance.

The rank matrix in figure 3a makes the distinction between uncertainty and instability visible. Precuneus probability is concentrated at rank 1, angular-gyrus probability at ranks 1–3, and cerebellar probability at ranks 6–7. Middle temporal and anterior cingulate regions have broader distributions because their relative positions depend on which evidence dimension receives emphasis. The ablation display in figure 3b confirms that every three-criterion score remains strongly concordant with the complete ordering. This agreement supports interpretation of a regional hierarchy while discouraging fine distinctions among the middle-ranked regions.

3.3. Posterior concentration and anatomical spacing

Under equal weights, precuneus, angular gyrus, and bilateral middle temporal gyri accounted for 70.54% of summed regional evidence. Across random weights, the median posterior share was 70.79%, and the central 95% interval was 64.47–75.76%. The lower bound remained well above 50%, satisfying the primary concentration hypothesis even when preference weights varied widely. The interval width of 11.29 percentage points indicates some dependence on how the four properties are valued, but no admissible region ordering implied an evenly distributed pattern.

The distribution in figure 4a is unimodal and centered near 0.71, so the posterior conclusion does not arise from two incompatible regions of preference space. The distance matrix in figure 4b adds anatomical context. Angular gyrus is relatively close to left middle temporal cortex and precuneus, whereas the two middle temporal peaks are far apart across hemispheres. Anterior cingulate is distant from the posterior and cerebellar peaks, and right cerebellum is remote from several cortical loci. These distances explain why centrality contributes information that neither effect magnitude nor extent contains. They also prevent the term “posterior core” from being interpreted as a single contiguous cluster: it denotes a distributed set of regions with convergent evidence.

3.4. Demographic and decision-balance analyses

The reconstructed Welch test showed that patients were 3.99 years younger than controls (95% CI -6.25 to -1.73), $t(242.46) = -3.484$, $p = 0.000586$. The standardized difference was Hedges $g = -0.430$ (95% CI -0.677 to -0.184). Education differed by 0.20 years (95% CI -0.44 to 0.84), $t(256.96) = 0.613$, $p = 0.540$, with $g = 0.076$ (95% CI -0.168 to 0.320). Thus, education was well balanced but age was not. The age result differs from an interpretation based solely on the printed group-comparison probability and is internally consistent with the reported means, standard deviations, and sample sizes.

Table 3. Weight and ablation robustness.

Region	Win (%)	Top three (%)	Mean rank
Precuneus	79.37	100.00	1.23
Angular-L	20.02	92.69	2.04
Middle temporal-L	0.00	59.36	3.58
Middle temporal-R	0.00	23.47	4.12
Anterior cingulate	0.00	13.63	4.91
Fusiform-L	0.61	10.86	5.26
Cerebellum-R	0.00	0.00	6.86

Excluded criterion	Spearman ρ
Attenuation	0.883
Extent	0.982
Classification	0.964
Centrality	0.893

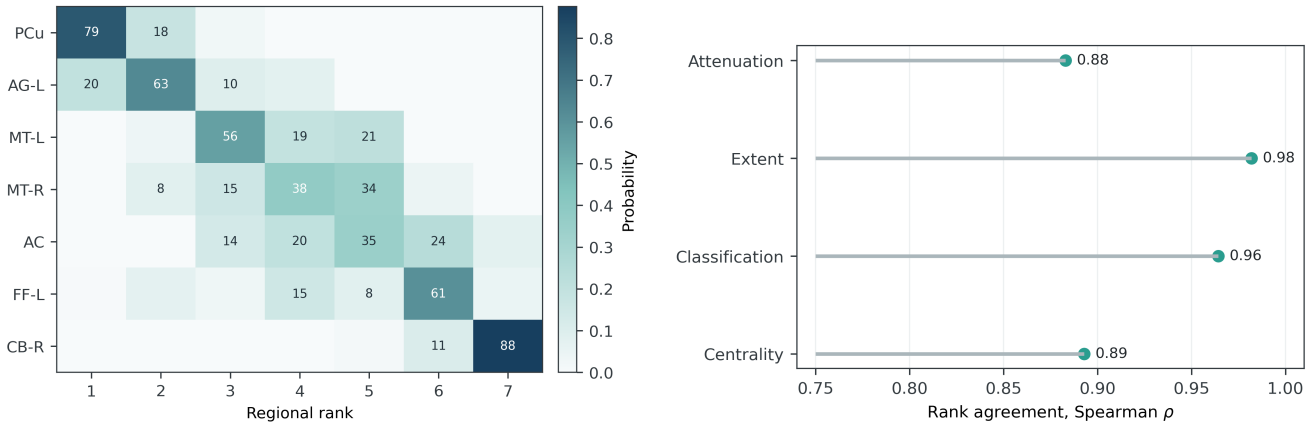

(a) Rank probabilities.

(b) Criterion ablation.

Figure 3. Robustness of regional ordering.

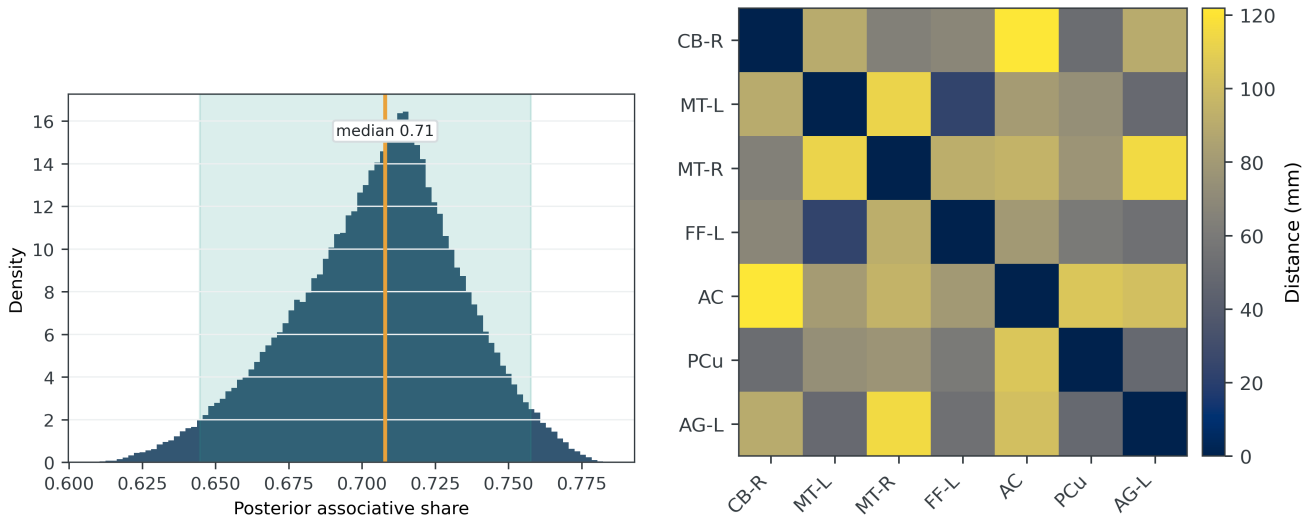

(a) Posterior evidence share.

(b) Peak-to-peak distance.

Figure 4. Posterior concentration and spatial relations.

Precuneus sensitivity was 91.60% and specificity 54.69%, yielding balanced accuracy of 73.145% and Youden $J = 46.29$ percentage points. Angular-gyrus sensitivity was 93.89% and specificity 52.34%, yielding balanced accuracy of 73.115% and Youden $J = 46.23$. Differences in balanced accuracy and Youden index were only 0.03 and 0.06 percentage points. The two regions therefore have virtually equal decision balance even though angular gyrus favors sensitivity more strongly and precuneus preserves slightly better specificity.

The confidence intervals in figure 5a separate the age and education conclusions clearly: only age excludes a negligible difference. The decision dots in figure 5b show why reporting accuracy alone is insufficient. Both posterior candidates identify most patients, but each labels many controls as patients. In a screening context, such a profile may be useful only as one component of a broader assessment; in a confirmatory diagnostic context, specificity near 53–55% would be inadequate. This asymmetry limits clinical claims even though the regional ordering itself is robust.

4. DISCUSSION

The study asked whether regional ALFF findings converge on a stable distributed phenotype and whether that phenotype is concentrated in posterior association cortex. Both parts were supported. Bilateral precuneus and left angular gyrus occupied the first two equal-weight positions, captured 99.4% of all rank-1 outcomes across 200,000 weight draws, and were joined by bilateral middle temporal regions in a posterior subset that retained roughly 65–76% of total evidence under widely varying preferences. The conclusion is therefore more specific than a list of attenuated regions: spontaneous signal reduction is organized around posterior systems that contribute to internally directed representation, semantic construction, memory, and the attribution of meaning.

The precuneus led because it combined four favorable properties rather than excelling on only one. Its $|t|$ value was greatest, its cluster was large, its peak accuracy tied for greatest, and its position was central within the seven-peak constellation. This convergence distinguishes regional salience from voxelwise significance. A cluster can be statistically strong yet spatially isolated, or extensive yet weak in decision balance. The precuneus was neither. Its anatomical role provides a plausible interpretation. Medial parietal cortex participates in constructing self-referential and episodic content and in coordinating shifts between internally and externally oriented cognition. Reduced resting amplitude may indicate a narrower dynamic range or altered local synchrony, either of which could constrain communication with lateral parietal and temporal association cortex. ALFF alone cannot identify the cellular mechanism, but the topology result shows where multimodal follow-up would be most efficient.

The angular gyrus formed the second component of the posterior core. It contained the largest cluster and achieved the same peak accuracy as the precuneus, but lower attenuation magnitude and centrality reduced its combined score. Its 20.0% win probability is not evidence against importance; rather, it quantifies the preferences under which angular-gyrus extent and sensitivity outweigh the stronger precuneus contrast. Functionally, the left angular gyrus is positioned to integrate semantic, episodic, auditory, and attentional information. Schizophrenia symptoms such as loose association, anomalous salience, and auditory hallucination may emerge when internally generated representations are assembled without reliable contextual constraints. The present regional pattern is compatible with that possibility because angular-gyrus attenuation occurs together with bilateral middle temporal and medial parietal abnormalities.

The middle temporal findings broaden the interpretation beyond a two-node account. Left middle temporal gyrus ranked third and entered the top three in 59.4% of weight draws; the right homologue ranked fourth and entered the top three in 23.5%. Their bilateral presence suggests that the phenotype is not simply a left-lateralized language abnormality. At the same time, the higher left-region score is consistent with stronger semantic and lexical specialization in the dominant hemisphere. The large interhemispheric distance in the MNI matrix further shows that bilateral labeling should not be mistaken for anatomical proximity. Future individual-level work can test whether reduced amplitude in the two temporal regions covaries within participants and whether that covariance relates to hallucination form, thought disorder, or verbal learning.

Anterior cingulate, fusiform, and cerebellar findings remained meaningful but did not define the leading pattern. Anterior cingulate cortex had strong attenuation but intermediate extent, accuracy, and centrality ranks. Its location outside the posterior concentration may represent an anterior regulatory disturbance that interacts with posterior representational systems. Left fusiform gyrus was unusual: it ranked sixth under equal weights but won 0.61% of random weight draws because its spatial centrality was high. This result is a useful warning against treating a rare win as stable dominance. Right cerebellum ranked last and never entered the top three, yet its attenuation can still matter biologically. Cerebellar contributions to timing, prediction, and cognitive coordination may be secondary within this regional constellation or may be underestimated by a method based on peak proximity in MNI space.

The weighting experiment is central to interpretation. Regional synthesis often hides value judgments by selecting one preferred statistic or by standardizing and averaging without testing alternatives. Sampling the simplex made those judgments visible. Precuneus dominance persisted across most combinations, and the posterior share never approached an even division. Criterion ablation produced correlations of 0.883–0.982 with the com-

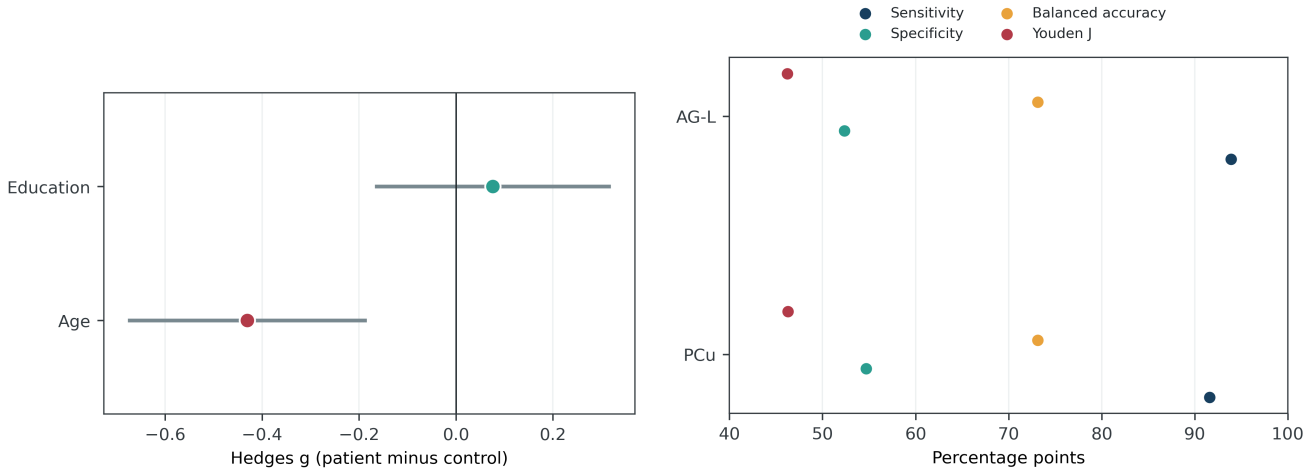

(a) Demographic effects.

(b) Posterior decision balance.

Figure 5. Inferential qualification.

plete ranking, showing that no single dimension carried the conclusion. Extent contributed the least unique ordering information, whereas attenuation and centrality altered ranks more noticeably. These observations justify reporting both the equal-weight scores and the preference distributions. A single ranking is convenient; the distribution shows how strongly it should be trusted.

The method also changes the meaning of regional classification values. Peak accuracy was only one quarter of the equal-weight score, and it was treated as a property of a region rather than proof of a deployable test. Precuneus and angular gyrus had nearly identical balanced accuracy and Youden index. Their high sensitivities were paired with specificities near chance, meaning that many healthy participants would receive a positive decision. This imbalance may be acceptable for an early research screen if followed by a more specific assessment, but it is not sufficient for diagnostic substitution. Moreover, the available accuracy values do not provide foldwise dispersion, calibration, decision-curve benefit, or external-site transport. Those omissions prevent strong claims about clinical utility.

The demographic audit revealed a second constraint. Recalculation from the printed summaries showed a statistically and practically meaningful age difference. Although age was entered as a voxelwise covariate, adjustment does not guarantee that the regional ranking is invariant to functional form or group-by-age interaction. Resting amplitude changes across adulthood, and different regions may have different age trajectories. If age relates more strongly to posterior than anterior ALFF, the observed concentration could be inflated or attenuated. The next decisive analysis should therefore use participant-level age residualization fitted within each training fold, inspect nonlinear terms, and repeat the ranking within an age-overlap subset. The present paper does not simulate those unavailable individual associations.

Motion is another concern. Rescanning participants who exceeded 2 mm or 2° limits removed gross movement, and framewise displacement entered the group model. Nevertheless, subthreshold motion can remain related to diagnosis and age. The combination of temporal filtering, nuisance regression, and spatial smoothing can also redistribute motion-related variance. A future implementation should report group distributions of mean framewise displacement, censor high-motion volumes, compare several validated denoising strategies, and demonstrate that posterior ranks survive those choices. Such checks are especially important because precuneus and angular-gyrus signals lie near regions susceptible to global and physiological influences.

Spatial inference must likewise be considered. Gaussian random-field cluster correction with a primary threshold of $p < 0.01$ produced the seven regions. Cluster extent depends on smoothing, smoothness estimation, and threshold selection; therefore, voxel counts are not immutable anatomical quantities. The present strategy reduced this vulnerability by log-transforming extent, converting it to a percentile, assigning it only one quarter of equal-weight evidence, and showing that removal of extent barely changed the ordering. The result is reassuring but not equivalent to recomputing the maps with permutation testing. When statistical images are available, nonparametric cluster control and threshold-free methods should be compared, and the regional score should be recalculated for each inferential choice.

Several strengths distinguish the analysis. The research question concerns distributed organization rather than a search for one diagnostic locus. Every numerical transformation is explicit, and the full code and intermediate tables accompany the manuscript. The use of percentile criteria prevents differences in physical units from dominating. Weight uncertainty converts an arbitrary modeling choice into a reported distribution. Criterion ablation identifies dimensions that matter for ordering. The de-

mographic audit checks internal arithmetic rather than accepting printed probability values, and the decision analysis prevents sensitivity from being interpreted without specificity. Finally, the spatial kernel is deliberately modest: it encodes proximity among observed peaks without claiming tractography or causal interaction.

The study also has clear limitations. Seven rows are sufficient for a transparent regional comparison but not for fitting a complex model. Percentile scores are coarse and depend on which regions pass the initial threshold. Coordinates represent cluster peaks rather than full shapes, and Euclidean proximity does not respect cortical folding, white-matter paths, or polysynaptic relations. Peak classification accuracy may be optimistic if feature selection and tuning were not fully nested. Medication exposure, single-site recruitment, and diagnostic composition restrict generalizability. Symptom correlations were absent in the clinical investigation, so the posterior score cannot be assigned to a specific symptom dimension. The photorealistic acquisition panel depicts the procedure generically and is not a participant photograph; all quantitative panels are generated directly from the included values.

These limitations define a focused validation agenda. A preregistered multisite study should acquire harmonized rs-fMRI, retain drug-naive and medicated strata, and measure hallucinations, thought disorder, semantic performance, episodic memory, and social cognition separately. The topology score should be calculated within each training partition, including voxelwise feature definition, nuisance modeling, and weight selection. Geodesic cortical distance, tractography-weighted distance, and functional covariance can then replace or complement Euclidean proximity. External validation should report calibration, balanced accuracy, predictive values at clinically relevant prevalence, and decision consequences. Longitudinal scans can test whether the posterior score is stable, treatment-sensitive, or prognostic.

The biological interpretation should remain proportionate to the measurement. Lower ALFF indicates reduced amplitude of slow blood-oxygen-level-dependent fluctuation within the selected frequency band. It does not by itself demonstrate neuronal inhibition, synaptic loss, or diminished information content. Medication, vascular physiology, arousal, respiration, and motion may alter the signal. Nevertheless, convergence across precuneus, angular, and middle temporal regions is anatomically coherent and robust to the declared analytic preferences. That combination supports a hypothesis of impaired posterior associative integration that is sharper than a diffuse whole-brain account and more defensible than a single-region diagnostic claim.

5. CONCLUSION

The paper's research question was whether multiple regional properties converge on a stable schizophrenia-related attenuation architecture and whether that architecture is concentrated in posterior association cortex. The answer is yes. Precuneus and left angular gyrus dominate the regional ordering across nearly all evidence preferences, and the addition of bilateral middle temporal cortex raises the posterior share to approximately 71%, with a preference range that remains well above one half. This conclusion survives omission of any one criterion, demonstrating that it is not driven solely by effect magnitude, cluster extent, classification accuracy, or anatomical centrality.

The result does not establish an individual diagnostic test. Precuneus and angular-gyrus classifiers are highly sensitive but only modestly specific, and the patient–control age difference remains a credible confound despite covariate adjustment. The most defensible inference is therefore mechanistic and organizational: reduced slow resting activity in schizophrenia is preferentially arranged across medial and lateral posterior association regions that jointly support self-related representation, semantic integration, and memory. Future multisite participant-level studies should test this topology prospectively, model age and motion within resampling, and determine whether the posterior score explains cognition, symptoms, treatment response, or course.

BIBLIOGRAFIA / REFERENCES

1. Owen MJ, Sawa A, Mortensen PB. Schizophrenia. *Lancet*. 2016;388:86–97. doi:10.1016/S0140-6736(15)01121-6.
2. Kahn RS, Sommer IE, Murray RM, Meyer-Lindenberg A, Weinberger DR, Cannon TD, et al. Schizophrenia. *Nat Rev Dis Primers*. 2015;1:15067. doi:10.1038/nrdp.2015.67.
3. Tandon R, Gaebel W, Barch DM, Bustillo J, Gur RE, Heckers S, et al. Definition and description of schizophrenia in the DSM-5. *Schizophr Res*. 2013;150:3–10. doi:10.1016/j.schres.2013.05.028.
4. Falkai P. A desperate search for biomarkers in schizophrenia: what is going wrong? *World Psychiatry*. 2011;10:38–39. doi:10.1002/j.2051-5545.2011.tb00011.x.
5. McCutcheon RA, Krystal JH, Howes OD. Dopamine and glutamate in schizophrenia: biology, symptoms and treatment. *World Psychiatry*. 2020;19:15–33. doi:10.1002/wps.20693.
6. Stephan KE, Friston KJ, Frith CD. Dysconnection in schizophrenia: from abnormal synaptic plasticity to failures of self-monitoring. *Schizophr Bull*. 2009;35:509–527. doi:10.1093/schbul/sbn176.
7. Uhlhaas PJ, Singer W. Abnormal neural oscillations and synchrony in schizophrenia. *Nat Rev Neurosci*. 2010;11:100–113. doi:10.1038/nrn2774.
8. Kühn S, Gallinat J. Resting-state brain activity in schizophrenia and major depression: a quantitative meta-analysis. *Schizophr Bull*. 2013;39:358–365. doi:10.1093/schbul/sbr151.
9. Dong D, Wang Y, Chang X, Luo C, Yao D. Dysfunction of large-scale brain networks in

schizophrenia: a meta-analysis of resting-state functional connectivity. *Schizophr Bull*. 2018;44:168–181. doi:10.1093/schbul/sbx034.
10. Whitfield-Gabrieli S, Thermenos HW, Milanovic S, Tsuang MT, Faraone SV, McCarley RW, et al. Hyperactivity and hyperconnectivity of the default network in schizophrenia and in first-degree relatives. *Proc Natl Acad Sci USA*. 2009;106:1279–1284. doi:10.1073/pnas.0809141106.
11. Sheffield JM, Barch DM. Cognition and resting-state functional connectivity in schizophrenia. *Neurosci Biobehav Rev*. 2016;61:108–120. doi:10.1016/j.neubiorev.2015.12.007.
12. Buckner RL, Andrews-Hanna JR, Schacter DL. The brain's default network: anatomy, function, and relevance to disease. *Ann N Y Acad Sci*. 2008;1124:1–38. doi:10.1196/annals.1440.011.
13. Raichle ME. The brain's default mode network. *Annu Rev Neurosci*. 2015;38:433–447. doi:10.1146/annurev-neuro-071013-014030.
14. Cavanna AE, Trimble MR. The precuneus: a review of its functional anatomy and behavioural correlates. *Brain*. 2006;129:564–583. doi:10.1093/brain/awl004.
15. Seghier ML. The angular gyrus: multiple functions and multiple subdivisions. *Neuroscientist*. 2013;19:43–61. doi:10.1177/1073858412440596.
16. Binder JR, Desai RH, Graves WW, Conant LL. Where is the semantic system? A critical review and meta-analysis of 120 functional neuroimaging studies. *Cereb Cortex*. 2009;19:2767–2796. doi:10.1093/cercor/bhp055.
17. Alderson-Day B, McCarthy-Jones S, Fernyhough C. Hearing voices in the resting brain: a review of intrinsic functional connectivity research on auditory verbal hallucinations. *Neurosci Biobehav Rev*. 2015;55:78–87. doi:10.1016/j.neubiorev.2015.04.016.
18. Zou QH, Zhu CZ, Yang Y, Zuo XN, Long XY, Cao QJ, et al. An improved approach to detection of amplitude of low-frequency fluctuation for resting-state fMRI: fractional ALFF. *J Neurosci Methods*. 2008;172:137–141. doi:10.1016/j.jneumeth.2008.04.012.
19. Jia XZ, Sun JW, Ji GJ, Liao W, Lv YT, Wang J, et al. Percent amplitude of fluctuation: a simple measure for resting-state fMRI signal at single voxel level. *PLoS One*. 2020;15:e0227021. doi:10.1371/journal.pone.0227021.
20. Li A, Zalesky A, Yue W, Howes O, Yan H, Liu Y, et al. A neuroimaging biomarker for striatal dysfunction in schizophrenia. *Nat Med*. 2020;26:558–565. doi:10.1038/s41591-020-0793-8.
21. Li H, Ou Y, Liu F, Su Q, Zhang Z, Chen J, et al. Region-specific insular volumetric decreases in drug-naive, first-episode schizophrenia and their unaffected siblings. *Am J Med Genet B Neuropsychiatr Genet*. 2020;183:106–112. doi:10.1002/ajmg.b.32765.
22. Li H, Ou Y, Liu F, Chen J, Zhao J, Guo W, et al. Reduced connectivity in anterior cingulate cortex as an early predictor for treatment response in drug-naive, first-episode schizophrenia. *Schizophr Res*. 2020;215:337–343. doi:10.1016/j.schres.2019.09.003.
23. Gong J, Wang J, Luo X, Chen G, Huang H, Huang R, et al. Abnormalities of intrinsic regional brain activity in first-episode and chronic schizophrenia: a meta-analysis of resting-state functional MRI. *J Psychiatry Neurosci*. 2020;45:55–68. doi:10.1503/jpn.180245.
24. Yu XM, Qiu LL, Huang HX, Zuo X, Zhou ZH, Wang S, et al. Comparison of resting-state spontaneous brain activity between treatment-naive schizophrenia and obsessive-compulsive disorder. *BMC Psychiatry*. 2021;21:544. doi:10.1186/s12888-021-03554-y.
25. Li P, Zhou M, Yan W, Du J, Lu S, Xie S, et al. Altered resting-state functional connectivity of the right precuneus and cognition between depressed and non-depressed schizophrenia. *Psychiatry Res Neuroimaging*. 2021;317:111387. doi:10.1016/j.pscychresns.2021.111387.
26. Niznikiewicz M, Donnino R, McCarley RW, Nestor PG, Iosifescu DV, O'Donnell B, et al. Abnormal angular gyrus asymmetry in schizophrenia. *Am J Psychiatry*. 2000;157:428–437. doi:10.1176/appi.ajp.157.3.428.
27. Oertel-Knöchel V, Knöchel C, Matura S, Prvulovic D, Linden DEJ, van de Ven V. Reduced functional connectivity and asymmetry of the planum temporale in patients with schizophrenia and first-degree relatives. *Schizophr Res*. 2013;147:331–338. doi:10.1016/j.schres.2013.04.024.
28. Power JD, Barnes KA, Snyder AZ, Schlaggar BL, Petersen SE. Spurious but systematic correlations in functional connectivity MRI networks arise from subject motion. *NeuroImage*. 2012;59:2142–2154. doi:10.1016/j.neuroimage.2011.10.018.
29. Parkes L, Fulcher B, Yücel M, Fornito A. An evaluation of the efficacy, reliability, and sensitivity of motion correction strategies for resting-state functional MRI. *NeuroImage*. 2018;171:415–436. doi:10.1016/j.neuroimage.2017.12.073.
30. Woo CW, Krishnan A, Wager TD. Cluster-extent based thresholding in fMRI analyses: pitfalls and recommendations. *NeuroImage*. 2014;91:412–419. doi:10.1016/j.neuroimage.2013.12.058.
31. Nichols TE, Holmes AP. Nonparametric permutation tests for functional neuroimaging: a primer with examples. *Hum Brain Mapp*. 2002;15:1–25. doi:10.1002/hbm.1058.
32. Chang CC, Lin CJ. LIBSVM: a library for support vector machines. *ACM Trans Intell Syst Technol*. 2011;2:27. doi:10.1145/1961189.1961199.
33. Varoquaux G, Raamana PR, Engemann DA, Hoyos-Idrobo A, Schwartz Y, Thirion B. Assessing and tuning brain decoders: cross-validation, caveats, and guidelines. *NeuroImage*. 2017;145:166–179. doi:10.1016/j.neuroimage.2016.10.038.
34. Varoquaux G. Cross-validation failure: small sample sizes lead to large error bars. *NeuroImage*. 2018;180:68–77. doi:10.1016/j.neuroimage.2017.06.061.
35. Button KS, Ioannidis JPA, Mokrysz C, Nosek BA,

Flint J, Robinson ESJ, et al. Power failure: why small sample size undermines the reliability of neuroscience. *Nat Rev Neurosci*. 2013;14:365–376. doi:10.1038/nrn3475.

36. Scheinost D, Noble S, Horien C, Greene AS, Lake EMR, Salehi M, et al. Ten simple rules for predictive modeling of individual differences in neuroimaging. *NeuroImage*. 2019;193:35–45. doi:10.1016/j.neuroimage.2019.02.057.
37. Poldrack RA, Baker CI, Durnez J, Gorgolewski KJ, Matthews PM, Munafò MR, et al. Scanning the horizon: towards transparent and reproducible neuroimaging research. *Nat Rev Neurosci*. 2017;18:115–126. doi:10.1038/nrn.2016.167.
38. Marler RT, Arora JS. The weighted sum method for multi-objective optimization: new insights. *Struct Multidiscip Optim*. 2010;41:853–862. doi:10.1007/s00158-009-0460-7.
39. Borgatti SP. Centrality and network flow. *Soc Networks*. 2005;27:55–71. doi:10.1016/j.socnet.2004.11.008.
40. Lakens D. Calculating and reporting effect sizes to facilitate cumulative science: a practical primer for t tests and ANOVAs. *Front Psychol*. 2013;4:863. doi:10.3389/fpsyg.2013.00863.
41. Gao Y, Tong X, Hu J, Huang H, Guo T, Wang G, et al. Decreased resting-state neural signal in the left angular gyrus as a potential neuroimaging biomarker of schizophrenia: an amplitude of low-frequency fluctuation and support vector machine analysis. *Front Psychiatry*. 2022;13:949512. doi:10.3389/fpsyt.2022.949512.